Preparation of a miR-155-activating Nucleic Acid Nanoflower to Study the Molecular Mechanism of miR-155 in Inflammation

Wenxin Wang
Huaqiao University
Jie Geng
Huaqiao University
Xiaohan Wu
Huaqiao University
Jianguang Zhang
Huaqiao University
Chenna Zheng
Quanzhou Medical College
Huachun Rao
Quanzhou Medical College
Chaochen Xu
Quanzhou Medical College
Tianyu Li
Huaqiao University
Yong Diao
Huaqiao University
Huiyong Yang (shyhy@hqu.edu.cn)
Huaqiao University

Research Article

Keywords: Nucleic acid nanoflowers, miR-155, RNA activation, inflammation

Posted Date: December 6th, 2021

DOI: https://doi.org/10.21203/rs.3.rs-1133989/v1

Abstract

Background

At present, the molecular mechanisms underlying inflammation remain unclear. In recent years, research on inflammation has focused on stimulating cell inflammation by using external pathogens such as LPS or inflammatory factors. To investigate the molecular mechanism of inflammation from a new perspective, we designed a nucleic acid nanoflowers (NFs) complex to directly activate inflammatory genes to study the inflammatory response without the need for external microbial factors to trigger an inflammatory response.

Results

An RNAa-type target gene-activated NF was designed. Human umbilical vein endothelial cells (HUVECs) were transfected with NFs carrying saRNAs to directly co-activate microRNA (miR)-155 and SHIP1 genes. Inflammatory gene and protein expression in the HUVECs were evaluated to assess whether miR-155 overexpression can trigger inflammation. After RNAa-type NFs were transferred into HUVECs, the expression of miR-155 and pro-inflammatory and cancer-related factors increased, anti-inflammatory factors were reduced, cell proliferation increased, and cell migration was promoted. IL-1β protein levels were decreased and SHIP1 expression was downregulated. When miR-155 and its target SHIP1 were both activated, the expression of both was unaltered, maintaining cell homeostasis.

Conclusion

MiR-155 and its target genes act as a molecular switch role in the development of inflammation.

Introduction

Inflammation, a defensive response of living tissues to damage, involves the vascular system. Vascular endothelial cells (VECs) form the inner single-cell layer that lines all blood vessels. Vascular endothelial growth factor (VEGF) participates in the regulation and generation of new blood vessels through its specific effects on vascular endothelial cells. Binding of VEGF to its receptor (VEGF-R) on endothelial cells results in a signal transduction cascade, the release of growth- and inflammatory factors, and, ultimately, endothelial cell proliferation and migration. These processes eventually produce a large number of new blood vessels that operate as a physical barrier between the blood and tissues [1]. They can rapidly secrete various active substances to regulate cardiovascular function, and at inflammatory sites, they can synthesize and secrete chemotactic factors such as IL-8 and MCP-1 to attract leukocytes [2, 3, 4]. Vascular proliferation can promote a variety of inflammatory and malignant diseases. Changing from short- to long-term inflammatory responses can result in the breakdown of immune tolerance and lead to major physiological changes of tissues, organs, and normal cells, thus increasing the risk of non-communicable diseases in the young and elderly. Long-term inflammation is also a contributory factor in the increase in morbidity and mortality of many degenerative diseases. The precise molecular mechanisms underlying inflammation remain unclear [5]. To date, studies investigating the mechanisms underlying inflammation have largely used inflammation-stimulating factors, such as lipopolysaccharides (LPS), to stimulate target cells and induce inflammatory responses [6, 7, 8, 9, 10, 11, 12, 13].

MicroRNAs (miRNAs) are endogenous, small (20–25 nucleotides), non-coding RNA molecules. MiRNA genes lie in intron regions of the genome and exon regions of non-coding genes. MiRNAs are transcribed from their host genes. They are involved in post-transcriptional gene regulation by binding directly to specific mRNA targets [14, 15, 16]. Each miRNA can regulate multiple genes, and multiple miRNAs can act synergistically to regulate the same gene [17, 18, 19]. MiRNAs are involved in the regulation of multiple immune responses, including the proliferation and differentiation of neutrophils and T and B cells, and in disease onset and development [20, 21, 22, 23]. When the body is in a state of chronic inflammation, miRNA expression becomes dysregulated [24, 25]. The dysregulation of miRNA expression contributes to disease development and malignant transformation [26, 27]. By regulating target gene expression, miRNAs can participate in the onset and development of various diseases, such as cancer and inflammation [28, 29]. It has become a potential candidate target for the treatment and prevention of a wide range of human diseases. miR-155 is a classic inflammatory miRNA [30]. It is highly expressed in immune cells that

infiltrate the diseased tissue [31]. Overexpression of miR-155 can lead to the release of pro-inflammatory cytokines and the downregulation of anti-inflammatory factors, whereas negative feedback regulates signal transduction to promote the continuation of inflammation [32]. Previous research has demonstrated that miR-155 is involved in the inflammatory response, but they have not paid attention to its source. If there is no external inflammatory substance stimulation, only increasing the expression of miR-155, can it cause inflammation?

RNA interference (RNAi) technology is widely used for the regulatory control of RNA expression. In 2006, Li et al. [33] discovered that small, double-stranded RNAs complementary to a gene promoter can specifically activate the expression of downstream genes. They termed this phenomenon RNA activation (RNAa). RNAa is a mechanism of gene activation mediated by small activating (sa)RNAs [34]. RNAa can be used to restore gene function by activating the expression of endogenous target genes and has considerable potential applications in gene regulation, and epigenetics, and as a novel gene therapeutic intervention. RNAa technology is straightforward and rapid to use; For example – a shorter experimental period and low experimental costs than traditional gene overexpression technology, which provides many advantages for its use in experimental exploration. Currently Dar et al. [35] have built an saRNA database (http://bioinfo.imtech.res.in/manojk/sarna/) for gene therapy research.

While RNAa has multiple advantages, similar to RNAi, the efficiency of saRNA delivery into cells is low. Currently, nucleic acid substances are mostly delivered into cells using viral or non-viral vectors as mediators. Viral vectors, such as adenoviruses and adeno-associated viruses, carry a risk for infection or have limited capacity, which limits their application. Non-viral vectors, mainly liposomes, are generally safe and have unlimited capacity, but their transfection efficiency is unsatisfactory and when used at high concentrations, they affect cell growth. Thus, an efficient and low-impact cell delivery system is urgently needed.

Recently, nucleic acid nanoflowers (NFs) have been developed for high-efficiency, non-toxic, and high-load nucleic acid delivery. Nucleic acid, as a biopolymer that stores genetic information in all organisms, has good biocompatibility and low immunogenicity and thus is a very suitable nanomaterial for use in vivo [36, 37]. NFs are prepared by rolling circle replication using a designed DNA template with embedded functional moieties and primers to generate concatemeric DNA [38]. NFs have an adjustable size and a large specific surface area. In comparison to DNA origami, NF sequence design is simple and NF preparation is facile and highly efficient. The use of NFs in biology has been studied extensively [39, 40, 41, 42]. RNA nanoparticles have become a research focus in the biomedical field. Lee et al. [43] prepared polymeric siRNA nanoparticles for tumor-targeted delivery based on rolling circle transcription. By designing DNA template sequences that can be amplified using the same amplification program, large quantities of saRNA sequences can be synthetized in vitro in a relatively short time.

In this study, the saRNA sequence that has been reported (number: VEGF-706) to effectively activate the expression of related genes is used. We embedded the saRNA in the designed linear template of rolling circle replication (RCT), optimized the reaction system and identified the best reaction system for the RCT process; we used different methods to transfer NFs into cells to compare the most stable and effective method for cell entry. Finally, the expression of the target gene *VEGF* was detected, which proved the applicability of the linear template we designed. The template, optimized reaction system, and cell entry method were used in the design of NFs that activate miR-155. These can activate the expression of miR-155 without the need for external microbial factors to trigger an inflammatory response and facilitate the exploration of the role of miR-155 in inflammation. We designed different DNA templates and used a single amplification scheme to synthesize a large amount of NF-RNAa sequence complexes in vitro in a short time. The complexes were optimized to allow highly efficient nucleic acid delivery into target cells. Upon activation of miR-155 expression in the cells, we evaluated the expression of inflammatory genes and analyzed the effect of miR-155 activation on the initiation, transformation, and progression of inflammation.

Results

Production and characterization of the nucleic acid NFs

Based on information in the saRNA database and reports by Guo and Chen [40, 41], we designed a linear DNA template (named L-T, with a phosphate group at the 5' end) complementary to the T7 promoter primer (Table S1) with embedded sense and

antisense saRNA sequences (termed *VEGF*-706) that can effectively activate VEGF expression (Figure 1A). Which proved that the usability of the linear template we designed and can be used to activate the miR-155 NFs.

The saRNAs were designed according to a report by Li et al33. We searched for the sequence of the host gene, MiR155HG, and 10,000 bases upstream of the 5′ end of the first exon in databases such as NCBI (https://www.ncbi.nlm.nih.gov/gene/?term=) and UCSC (https://genome.ucsc.edu/), and we predicted the transcription start site to be located at base 8,912 (Figure 1B) using various online resources (http://linux1.softberry.com/cgi-bin/programs/promoter/tssp.pl and http://www.bio-soft.net/sms/cpg_island.html). Next, we predicted the regions enriched in CpG islands to ensure that the designed saRNA avoids these regions (Figure 1C). We found that the region of 7,710–9,584 was enriched in CpG islands (Figure 1C). Therefore, the saRNA sense strand region of 7,712–8,712 was selected. We screened the sense strand region of the saRNA that can activate miR-155. Finally, seven eligible saRNAs were screened out (Table 1) and embedded into the template sequence designed above (Table 2).

Table 1 Sequences in line with saRNA design principles

Gene name	Positive-sense strand	antisense strand
miR-155-1	GUC ACC UCA GCC UCC CAA A	CAG UGG AGU CGG AGG GUU U
miR-155-2	UAU CCC UCU UAG UCU GCU A	AUA GGG AGA AUC AGA CGA U
miR-155-3	GUC UGC UAG GGU UGC CAU A	CAG ACG AUC CCA ACG GUA U
miR-155-4	AUA GAC UGG AUG GCU GAU A	UAU CUG ACC UAC CGA CUA U
miR-155-5	ACA UUC UGG AGG CUA GAA A	UGU AAG ACC UCC GAU CUU U
miR-155-6	GGA CUC UCU UCC UGG CUU A	CCU GAG AGA AGG ACC GAA U
miR-155-7	UCU UCC UGG CUU ACA GGA A	AGA AGG ACC GAA UGU CCU U

Table 2 Template and primer sequence for preparing nucleic acid nanoflowers that can activate miR-155

name	Sequence（5’→ 3’）
Template-1	ATAGTGAGTCGTATTAACGTACCAACAAGTCACCTCAGCCTCCCAAAACTTGTTTGGGAGGCTGAGGTGACATCCCT
Template-2	ATAGTGAGTCGTATTAACGTACCAACAATATCCCTCTTAGTCTGCTAACTTGTAGCAGACTAAGAGGGATAATCCCT
Template-3	ATAGTGAGTCGTATTAACGTACCAACAAGTCTGCTAGGGTTGCCATAACTTGTATGGCAACCCTAGCAGACATCCCT
Template-4	ATAGTGAGTCGTATTAACGTACCAACAAATAGACTGGATGGCTGATAACTTGTATCAGCCATCCAGTCTATATCCCT
Template-5	ATAGTGAGTCGTATTAACGTACCAACAAACATTCTGGAGGCTAGAAAACTTGTTTCTAGCCTCCAGAATGTATCCCT
Template-6	ATAGTGAGTCGTATTAACGTACCAACAAGGACTCTCTTCCTGGCTTAACTTGTAAGCCAGGAAGAGAGTCCATCCCT
Template-7	ATAGTGAGTCGTATTAACGTACCAACAATCTTCCTGGCTTACAGGAAACTTGTTCCTGTAAGCCAGGAAGAATCCCT
T7	TAATACGACTCACTATAGGGAT

Note: All the above sequences (except T7) need to modify the phosphate group at the 5'end

We optimized the template concentration (Figure 2A), primer concentration ratio (Figure 2B), ligase, optimized hybridization time and ligation time (Figure 2C-E), and raw material concentration (Figure 2F). The optimized result is shown in Figure 2G-H. It was finally determined that the ratio of template concentration to primer concentration was 1:1 in subsequent experiments, and T4

DNA ligase was used for the ligation reaction. The hybridization time was 2h, the ligation time was 3h, and the rNTP concentration was 2mM. As shown in Figure 2I-J, we have successfully prepared nucleic acid nanoflowers, which are of homogenous sizes and shapes, and the size is nanoscale.

The results of gel imaging of the PEI-NF complexes are shown in Figure 3A. According to lanes 1 and 2 in the figure, PEI and the nucleic acids interact via electrostatic interaction to form a positively charged complex, and the surface charge is reduced. Therefore, the target band does not migrate downward. When only PEI is present, bright bands do not appear in the absence of nucleic acids. Thus, the PEI-NF complex was successfully prepared.

PEI-NF complex and saRNA that can activate *VEGF* expression have no effect on cell activities

The cytotoxicity of the PEI-NF complexes towards HUVECs was evaluated by CCK-8 assays (Figure 3B). The survival rate of HUVECs treated with PEI-NFs or saRNA was >1, and there was no significant difference with the control group ($P > 0.05$). These results showed that neither the PEI-NFs nor the saRNA had cytotoxic effects on HUVECs. In addition, PEI-NFs and saRNA did not significantly suppress cell proliferation ($P > 0.05$). Thus, the PEI-NFs were further evaluated in subsequent experiments.

PEI-NFs that can activate *VEGF* expression successfully enter cells

Fluorescence microscopy confirmed the presence of PEI-NFs within the cells (Figure 3C). Cells stained with DAPI were imaged with an exposure time of 10 ms, and those stained with Cy3 were imaged with an exposure time of 100 ms. In the control group, no Cy3 fluorescence signal was detected, whereas in the experimental group (L-T), red fluorescence was observed, indicating that the PEI-NFs had successfully entered the cells. Flow cytometry was used to quantitatively evaluate the efficiency of PEI-NF delivery into the cells (Figure 3D, E). Compared with the control group, the efficiency of PEI-NF delivery into the cells was > 70% ($P < 0.0001$; Figure 3E).

PEI-NF complex and saRNA activate *VEGF* expression

We examined the activation of VEGF expression induced by PEI-NF complex and saRNA using RT-qPCR (Figure 3F). Compared with that in the control group, the relative expression of VEGF in the experimental group of cells treated with PEI-NFs or saRNA activated was increased by 2.5-fold ($P < 0.01$). This result showed that the PEI-NF complex and saRNA effectively activated VEGF expression. There was no difference in the relative VEGF expression between the PEI-NF- and saRNA-treated cells, indicating that they have similar efficiency. Thus, we confirmed that the nucleic acid NF was effective and could be used for the activation of miR-155.

Changes in the template sequences of miR-155-activating NFs have no impact on cell proliferation

In the above experiments, we screened seven saRNAs that can activate miR-155. We used the CCK-8 assay to detect the inhibitory effects of nucleic acid NFs M1–M7 prepared from seven different template sequences on cell proliferation at 12, 24, 48, and 72 h (Figure 4A). Compared with the control group, NFs M1–M7 had no inhibitory effect on cell proliferation even after 72 h ($P > 0.05$). Nearly all NFs had similar effects, and the cell survival rate remained nearly constant from 12 h to 24 h, slightly decreased between 24 h and 48 h, and decreased from 48 h to 72 h (to approximately 1). These findings showed that a change in the template sequence has no inhibitory effect on cell proliferation.

Screening of saRNAs that can activate *miR-155* expression

To screen for saRNAs that can activate miR-155, we evaluated the NFs M1–M7 for their capacity to activate MiR155HG expression (Figure 4B–D) and miR-155 expression (Figure 4E–G) in HUVECs after treatment for 12, 24, 48, or 72 h. Compared with that in the control group, relative MiR155HG gene expression in the experimental groups treated with M1–M7 significantly increased within 48 h ($P < 0.01$) and decreased between 48 h and 72 h. miR-155 expression increased over time. Based on the relative expression levels of miR-155, all seven saRNAs were found to activate miR-155 expression. M5 had the best effect; it enhanced miR-155expression level by 11.5-fold ($P < 0.001$) (Figure 4H). Therefore, this saRNA was used to activate miR-155 expression in further experiments.

NFs that can activate *miR-155* expression successfully enter cells

Using fluorescence microscopy, we confirmed the presence of NFs that can activate miR-155 within cells (Figure 5A). Cells stained with DAPI were imaged with an exposure time of 10 ms, and those stained with Cy3 were imaged with an exposure time of 100 ms. In the control group, no Cy3 fluorescence signal was detected, whereas in the experimental group (M5), red fluorescence was observed, indicating that the M5 NFs had successfully entered the cells.

Overexpression of miR-155 promotes the migration of HUVECs

Cell migration was detected by a scratch assay at 0 h,12 h, 24 h, 48 h, and 72 h after transfection of the cells (Figure 5B). All cells migrated over time, but compared with the control group, cells with activated miR-155 expression migrated faster, indicating that miR-155 overexpression promoted cell migration as indicated by scratch closure. This result preliminarily indicated that miR-155 overexpression may cause inflammation.

Activation of miR-155 affects the expression levels of key signaling molecules and inflammatory factors

In a preliminary experiment, we treated HUVECs with different concentrations of LPS and found that 0.1 μg/mL LPS effectively stimulated HUVECs; miR-155 expression first increased and then decreased, and the highest expression level was approximately 4-fold higher than that in the control group (Figure S2A). Treatment of cells with a high concentration of LPS caused apoptosis (Figure S2B–H). Next, we studied whether activated miR-155 can trigger an inflammatory response. We treated HUVECs with the miR-155-activating NFs for 72 h and used RT-qPCR to detect changes in the expression of inflammation-related effectors and signaling pathway genes (Figure 6A). After miR-155 activation, the relative expression levels of inflammation-related genes changed. Gene expression of the anti-inflammatory factor SHIP1 was significantly reduced ($P < 0.01$). Gene expression of the pro-inflammatory factors TNF-α, IFN-γ, IL-1β, IL-6, and FOXO3A was significantly increased ($P < 0.05$). IKKβ activity is related not only to inflammatory diseases, but also to cancer onset. IKKβ may act as an oncogene promoting malignant transformation and tumor progression. Our research showed that after miR-155 was activated, IKKβ gene expression was significantly increased ($P < 0.001$), suggesting that miR-155 activation may be related to cancer. The PI3K/AKT signaling pathway regulates multiple biological processes [46] and is closely related with tumor development and metastasis [47]. We found that PI3K/AKT gene expression increased after miR-155 activation ($P < 0.01$), which may be related to tumor development. NF-κB is a key transcription factor involved in inflammatory signaling pathways and responsible for the initiation of transcription of downstream inflammatory factors [48]. Activated miR-155 increased the expression of NF-κB ($P < 0.05$) as well as that of pro-inflammatory factors ($P < 0.05$), indicating the induction of an inflammatory response. Together, these results suggested that miR-155 overexpression is related to inflammation and tumorigenesis.

Activated miR-155 significantly upregulates IL-1β protein expression and downregulates SHIP1 protein expression

To verify that activation of miR-155 can induce inflammation, we treated HUVECs with miR-155-activating NFs for 72 h and then measured the expression of pro-inflammatory and anti-inflammatory proteins by western blotting. Compared with the control group, HUVECs treated with LPS or miR-155-activating NFs showed upregulated IL-1β protein expression and downregulated SHIP1 protein expression. However, compared with LPS, miR-155 activation had a significantly stronger promotive effect on IL-1β protein expression ($P < 0.05$, Figure 6B, C) and suppressive effect on SHIP1 protein expression ($P < 0.05$, Figure 6D, E). Thus, NF-M5 significantly induced the expression of the inflammatory factor IL-1β and reduced that of the negative regulator of inflammation, SHIP1. These results indicated that in the absence of exogenous inflammatory factors, NFs can directly activate miR-155 expression in cells and induce cell inflammation.

Prediction of miR-155 target genes and analysis of gene co-expression

We predicted the human target genes of miR-155 using four miR-155 target gene prediction tools and analyzed the enriched regions of the target genes involved in the inflammatory signaling. The predicted target genes are listed in Table S3. Although the numbers of target genes yielded by the different tools differed, there were a large number of common genes and only a few genes were predicted by only one tool. In total, 64 target genes were predicted by all four tools and thus had a high confidence (Figure 7A). Therefore, these genes were selected as the final miR-155 target genes. Next, we used the DAVID tool to analyze the

enrichment of these genes in signaling pathways, which revealed that the miR-155 target genes showed a distinct enrichment pattern. Forty-seven target genes were involved in 32 signaling pathways. There were eight groups of target genes involved in different inflammatory signaling pathways (Table S4), suggesting that miR-155 regulates inflammatory signal transmission by targeting these genes to ultimately regulate the onset and development of inflammation. The PI3K-AKT pathway was enriched in miR-155 target genes. Our previous studies showed that the expression of the effectors SHIP1 and FOXO3A changed significantly after the activation of miR-155 expression (Figure S2B). This indicates that miR-155 may promote PI3K-AKT signaling by inhibiting the expression of SHIP1, thereby causing inflammation.

Co-expression of miR-155 with its target SHIP1 cancels out their individual effects, suppressing inflammation

In the saRNA database, we did not find an saRNA that can activate SHIP1 expression. Therefore, according to the saRNA design principles reported by Li et al33, we searched the 5,000 bases upstream of the 5′ end of the SHIP1 gene, INPP5D, for the transcription start site (Figure 7B) and a region enriched in CpG islands. The transcription start site was at 1,911, and there was no region enriched in CpG islands. Therefore, the saRNA sense strand region (1–1,711) was selected. We screened out eight saRNAs that met all the conditions (Table S5), and embedded the selected sequences into the template sequence (Table S6). We used the same methods as those used above to prepare NFs that can activate SHIP1 expression. The CCK-8 assay was used to evaluate the inhibitory effects of nucleic acid NFs S1–S8 prepared from the eight template sequences on cell proliferation at 12 h, 24 h, 48 h, and 72 h (Figure 7C). Nucleic acid NFs S1–S8 had no inhibitory effect on cell proliferation in the first 48 h, but they did inhibit growth after 48 h ($P < 0.05$). All nucleic acid NFs had similar efficacy. This finding indicated that a change in SHIP1 expression affects cell proliferation and that SHIP1 expression is activated within 48 h to 72 h, inhibiting cell proliferation via the PI3K-AKT pathway.

Nucleic acid NFs S1–S8 activated SHIP1 expression after 72 h, as shown in Figure 7D. S7 was the most effective. We evaluated cell morphology after the activation of miR-155 expression, SHIP1 expression, and both in HUVECs (Figure 7E–H). In the presence of serum, the cell growth rate was high, and the cells were in good state and displayed long spindle-like morphology and tight connections (Figure 7E). After miR-155 activation, the cell growth rate increased compared to that of control cells, the cells were in a normal state, cell density increased, and cells were slightly overlapping (Figure 7F). Upon SHIP1 activation, the cell growth rate decreased, cell density was obviously reduced, and the cells showed a scattered distribution (Figure 7G), suggesting that SHIP1 expression enhanced apoptosis in HUVECs. When miR-155 and SHIP1 expression was activated simultaneously, the cell growth rate was comparable to that of control cells and the cell density was only slightly decreased, indicating a normal state (Figure 7H). Further, upon simultaneous activation of miR-155 and SHIP1, the expression of both genes did not change (Figure 7I). These findings indicated that upon simultaneous activation of miR-155 and SHIP1, their individual effects are canceled out, and inflammation would not be promoted.

Discussion

In this study, we first optimized the concentration ratio of template to primer, type of ligase, hybridization time, ligation time, and raw material concentration, and successfully prepared nucleic acid NFs with different rNTP concentrations. Using SEM, we found that the nucleic acid NFs had a petal-like shape and a size of approximately 200 nm, and were uniform in size. We found that the nucleic acid NFs did not inhibit cell proliferation and could enter cells with an efficiency of approximately 70%. The NFs could enhance VEGF expression by 2.5-fold. There was no difference with VEGF expression activation according to the protocol reported by Guo and Chen [40, 41].

Changes in the template sequences of the nucleic acid NFs had no inhibitory effect on cell proliferation. We screened out an saRNA sequence that could effectively activate miR-155, with sense strand ACA UUC UGG AGG CUA GAA A and antisense strand UGU AAG ACC UCC GAU CUU U. We inserted the selected saRNA into the template (T5) and prepared a nucleic acid NF (M5) to qualitatively detect its entry into the cell. The nucleic acid NF-M5 entered the cells and enhanced the expression of miR-155 by approximately 11-fold. By evaluating the cell migration ability and the expression of inflammation-related factors after treatment with the NFs, we found that miR-155 expression was activated by NF-M5 stimulation, which promoted cell proliferation. Further, the activation of miR-155 expression promoted cell migration. The overexpression of miR-155 led to

inflammation by activating the NF-κB signaling pathway, increasing the expression of pro-inflammatory factors, and inhibiting the expression of anti-inflammatory factors, and it also induced high expression of genes encoding tumor-related factors and genes involved in signaling pathways. Our findings preliminarily demonstrated that in the absence of exogenous inflammatory factors, direct activation of miR-155 expression can trigger cell inflammation and possibly, the occurrence and development of tumors. Further study showed that miR-155 overexpression upregulated IL-1β and downregulated SHIP1 protein expression. IL-1β is an important mediator of the inflammatory process [44]. It promotes the release of neutrophils from the bone marrow, induces chemotaxis of monocytes and multinucleated cells to infiltrate the inflammation site, and induces local release lysosomal enzymes [45, 46, 47]. SHIP1 serves as an inhibitor of inflammation and NF-κB activity [32]. It has been shown that miR-155, when upregulated in synovial tissue and synovial fluid macrophages, targets SHIP1, leading to increased levels of pro-inflammatory cytokines [48]. Thus, miR-155 can be regarded a switch molecule that triggers inflammation.

We explored the effect of co-expression of miR-155 and its target genes on inflammation. To this end, we first predicted and screened the target genes of miR-155. Upon co-expression of miR-155 and SHIP1, we found that miR-155 targeted SHIP1 and inhibited its expression, and SHIP1 promoted this effect of miR-155, so that ultimately, they canceled out each other's expression and effects, which is expected to suppress inflammation.

Materials And Methods

Cell culture

Human umbilical vein endothelial cells (HUVECs) (a friendly gift from Lin Junsheng, Huaqiao University School of Medicine) were cultured in high-glucose Dulbecco's modified Eagle's medium (Biological Industries) supplemented with 10% (v/v) heat-inactivated fetal bovine serum (Biological Industries) and 1% (v/v) antibiotic cocktail (100 U/ml penicillin, and 100 mg/ml streptomycin, Biological Industries) in an incubator at 37°C with 5% CO_2.

saRNA design

Based on information in the saRNA database and reports by Guo and Chen [49, 50], we designed a linear DNA template (named L-T, the 5′ end was modified with a phosphate group) that was complementary to the T7 promoter primer (named T7) with embedded sense and antisense saRNA sequences (termed VEGF-706) that can effectively activate VEGF expression. Sequence information for the primers used is provided in Table S1. The secondary structures of the products after 1 and 5 rolling circle transcription cycles were analyzed using the M-fold website (http://unafold.rna.albany.edu/?q=mfold) (Figure S1). We found that it is better to produce multiple stem-loop structures. All templates were synthetized at GenScript (Nanjing, China). saRNAs were designed according to a report by Li et al [33]. saRNAs that met all the inclusion criteria were selected and were embedded in the linear DNA template designed above to prepare nucleic acid NFs that can activate miR-155.

NFs production and characterization

The phosphorylated linear DNA template L-T and T7 Primer were mixed in 1× T4 DNA ligase (2001A, TaKaRa) buffer (66 mM Tris-HCl, 6.6 mM MgCl2, 10 mM DTT, 66 μM ATP, and 3.3 μM [32P]-Na4P2O7). The DNA was denatured at 95°C for 5 min and slowly cooled to room temperature to hybridize. Then, T4 DNA ligase was added at a final concentration of 10 U/μL to seal the nick of the linear template to form a circular template. The circular template (0.5 μM) was incubated with T7 RNA polymerase (5 U/μL; M025, BioLabs) in 1× T7 RNA polymerase buffer (40 mM Tris-HCl, 2 mM spermidine, 6 mM MgCl2, and 1 mM DTT) containing 2 mM rNTPs (4019, TaKaRa) and RNase Inhibitor (1 U/μL; R8060, Solarbio) at 37°C for 24 h for RNA transcription and synthesis. After the reaction, the temperature was increased to 65°C for 10 min to inactivate the polymerase. The reaction product was sonicated for 3 min to prevent polymerization and then centrifuged at 12,000 × g for 6 min. The supernatant was removed, and the pellet was resuspended in an equal volume of RNAse-free water to obtain purified NFs. To determine the NF concentration, the absorbance at 260 nm was measured. NF quality was assessed by 1% agarose gel electrophoresis. The samples were mixed with RNA loading buffer at a volume ratio of 4:1 and loaded on a gel. The electrophoresis conditions were 85 V, 200 A. The electrophoresis results were observed with a gel imaging system and images were captured.

Silicon (Si) wafers were soaked in aqua regia (3:1, H_2SO_4: HNO_3) overnight, rinsed with ethanol and acetone, and dried. The purified nucleic acid NFs were dropped onto the Si wafers using a micropipette. The wafers were dried in an oven at 60°C, gold-coated, and observed by scanning electron microscopy (SEM, Phenom) to examine NF morphology and size.

Polyethylenimine (PEI)-NF complex preparation

To ensure the stability of the NFs, we incubated the NFs (10 μL) with linear (L)PEI(LPEI, Mw=25000) diluted to 0.1 μg/μL in RNase-free water to form complexes (termed PEI-NFs) that can readily enter cells, at room temperature for 15 min. Binding was assessed by gel electrophoresis.

Cytotoxicity assay

Cells were seeded in 96-well plates at 5,000 cells/well. The wells were assigned to a blank group, control group, and experimental group, with three replicate wells for each group, and the plates were incubated in a 5% CO_2 incubator at 37°C for 24 h. Then, the cells were washed with PBS and the culture medium was replaced with 50 μL of fresh complete medium. PEI-NFs were added to the cultured cells and the plates were further incubated for 24 h. The cell counting kit-8 (C0038, Beyotime) assay was employed to detect cell viability. The experiment was repeated three times.

Fluorescence cell imaging

We modified the T7 promoter sequence at the 5′ end with the fluorophore Cy3 for fluorescent cell imaging to confirm NF penetration into the cells. Cells were seeded into 24-well culture plates at 1 × 105 cells/well and cultured in a 5% CO_2 incubator at 37°C for 24 h. PEI-NFs were added to the cells and the plates were further incubated for 24 h. Then, the cells were gently washed with PBS, fixed with 4% paraformaldehyde, permeabilized with 0.3% Triton X-100, and stained with DAPI(Beyotime). The stained cells were observed under an inverted fluorescence microscope (CKX41SF, OLYMPUS CORPORATION).

Flow-cytometric analysis of the efficiency of PEI-NF delivery into cells

HUVECs were seeded in 12-well plates at 1 × 105 cells/well. The cells were cultured in a 5% CO_2 incubator at 37°C for 24 h. The cells were washed with PBS, the medium was replaced with fresh medium, PEI-NFs were added, and the plates were incubated for 12 h. Then, the cells were digested into a single-cell suspension. After centrifugation, the cells were washed several times with PBS and resuspended in 1mL of PBS. Finally, the samples were subjected to flow cytometry.

Cell scratch assay of cell migration

HUVECs were seeded into a 6-well plate at 2×10^5 cells/well and incubated for 24 h. Then, the HUVECs were washed. Using a sterile 200-μL pipette tip, three scratches were made on each cell monolayer. The back of the 6-well plates were labeled with horizontal lines using marker pens for easy identification. The cells were washed twice, and complete medium was added. LPS and PEI-NFs were added to the cells. The scratches were evaluated at 12, 24, 48, and 72 h to compare the effects of the two treatments on cell migration capacity.

Real-time reverse transcription RT-qPCR analysis of gene expression

Cells were seeded in a 24-well plate at 5 × 104 cells/well. Wells were assigned to experimental groups and a control group. After 24 h of incubation, the PEI-NFs complexes were added. Total RNA was extracted at 12, 24, 48, and 72 h using an RNeasyTM Animal RNA Isolation Kit with spin columns (R0027, Beyotime) per the manufacturer's protocol. The RNA was reverse-transcribed using HiScript® Q RT SuperMix for qPCR (+gDNA wiper) (Vazyme). The cDNA was used for PCR amplification of *VEGF, MiR55HG*, inflammation-associated genes, and DAPDH. In addition, the RNA was reverse-transcribed using the miRNA 1st Strand cDNA Synthesis Kit (by stem-loop) (MR101-01/02, Vazyme), a stem-loop primer for miR-155, and a reverse primer for U6 for reverse transcription of miR-155 and U6, respectively, and the cDNA was used for PCR amplification of miR-155 and U6. The primers used for RT-qPCR are listed in Table S2. The primers were synthetized at Nanjing Genscript (Nanjing, China). RT-qPCRs were run using the two-step method. Relative expression levels were determined using the $2^{-\Delta\Delta Ct}$ method.

Western blotting

LPS/NF-stimulated cells in 6-well plates were washed twice with ice-cold PBS. The cells were lysed with 200 μL of high-efficiency RIPA tissue/cell lysis buffer (R0010, Solarbio) on ice for 20–30 mins. The lysates were centrifuged at 12,000 × g, 4°C for 5 min, and the supernatants were collected in centrifuge tubes and stored at −80°C. The total protein content was determined using an Enhanced BCA Protein Assay Kit (P0010S, Beyotime Biotechnology). Cell lysates containing 300 μg protein were mixed with 5× sample buffer (containing DTT), and heated at 99°C for 10 min. Then, the samples were separated by 12% SDS-PAGE at 70 V for 30 min followed by 120 V for 60 min and electroblotted on PVDF membranes at 300 mA for 1 h. The membranes were incubated in blocking solution (5% non-fat milk in TBST) at room temperature for 1 h. Then, the membranes were washed three times in TBST for 5 min each, incubated with primary antibodies (rabbit anti-SHIP1 polyclonal antibody, bs-3567R, Bioss and rabbit anti-GAPDH polyclonal antibody, bs-0755R, Bioss, diluted 1:1000 in TBST containing 5% BSA) at 4°C overnight, washed with TBST buffer three times for 5 min each, and incubated with goat anti-rabbit IgG-HRP (1:2000, KGAA35, Keygen BioTECH) at room temperature for 1 h. The membranes were washed three times with TBST buffer for 10 min each. The membranes were exposed using BeyoECL Plus (P0018S, Beyotime), and band intensities were quantified using the ImageJ software.

Prediction of miR-155 target genes and analysis of gene co-expression

We used four miR-155 target gene prediction tools, i.e., TargetScan (http://www.targetscan.org/vert_72/), miRanda (http://www.microrna.org/), PITA (https://pictar.mdc- berlin.de/), and picTar (https://pictar.mdc-berlin.de/), for miR-155 target gene prediction. For the predicted miR-155 target genes, we used the DAVID tool (https://david.ncifcrf.gov/tools.jsp) to analyze enriched signal pathways. The SHIP1 gene was selected, and miR-155 may promote PI3K-AKT signaling by inhibiting the expression of SHIP1, thereby causing inflammation. Thus, we designed nucleic acid NFs that can activate SHIP1 expression as described above to study its effect on miR-155 expression and explore the interaction between the miRNA and its target genes after activation.

Data analysis and statistics

Data are expressed as mean ± standard deviation. For comparisons of multiple groups, one-way analysis of variance was used. Differences between two groups were compared using t-tests. Data were analyzed using the SPSS or Prism software (version 6.02, GraphPad Software). $P < 0.05$ was considered statistically significant.

Conclusion

In this study, we evaluated whether miR-155 is an important molecular switch in the process of inflammation, using nucleic acid NF technology. We demonstrated that miR-155 causes inflammation by increasing the expression of pro-inflammatory factors and inhibiting the expression of anti-inflammatory factors. MiR-155 can interact with its target genes after co-expression and affect the onset and development of inflammation. This study provided a new research idea for the molecular switch of inflammation. In disease research, miR-155 can be used as a marker to assess whether the body has inflammation and can provide important information for early disease detection and warning.

Declarations

Acknowledgements

We greatly appreciate to Dr. Zhang Wei for his guidance on our work.

Authors' contributions

Experiments were designed by HY and YD and conducted by WW, JG, XW, CX and JZ. Data was analysed by WW, CZ and HR. Manuscript was prepared by WW and edited by HY, TL and YD. All authors read and approved the final manuscript.

Funding

Project of Science and Technology of Fujian Province of China [2019J05094, 2020NZ010008]. Research on the molecular mechanism of the occurrence and maintenance of uncontrollable inflammation based on the theory of "bistable", the basic operating expenses of central universities-Huaqiao University Young and Middle-aged Teachers Science and Technology Innovation Funding Program [ZQN-PY319]; Quanzhou Science and Technology Social Development Project [2020SY004]; Key projects of Quanzhou city[2018Z017].

Availability of data and materials

Data sharing is applicable to this article

Ethics approval and consent to participate

Not applicable

Consent for publication

All the co-authors were aware of this submission and approve for publication.

Competing interests

The authors declare that they have no competing interests.

Not applicable.

References

1. Philipp J, Le Gleut R, Toerne CV, et al. Radiation Response of Human Cardiac Endothelial Cells Reveals a Central Role of the cGAS-STING Pathway in the Development of Inflammation. Proteomes. 2020;8(4):30.
2. Hu C, Liu B, Xu Y, et al. EP3 Blockade Adds to the Effect of TP Deficiency in Alleviating Endothelial Dysfunction in Atherosclerotic Mouse Aortas. Front Physiol. 2019; 10:1247.
3. Ding T, Sun J. Mechanistic Understanding of Cell Recognition and Immune Reaction via CR1/CR3 by HAP- and SiO2-NPs. Biomed Res Int. 2020; 2020:7474807.
4. Chang H, Cao Y, Lin YI, et al. Association between toll-like receptor 6 expression and auxiliary T cells in the peripheral blood of pediatric patients with allergic purpura. Exp Ther Med. 2015;10(4):1536-1540.
5. Macejova D, Podoba J, Toporova L, et al. Causal associations of autoimmune thyroiditis and papillary thyroid carcinoma: mRNA expression of selected nuclear receptors and other molecular targets. Oncol Lett. 2019;18(4):4270-4277.
6. Vilmont V, Tourneur L, Chiocchia G. Fas-associated death domain protein and adenosine partnership: fad in RA. Rheumatology (Oxford). 2012;51(6):964-975.
7. Pauley KM, Satoh M, Chan AL, Bubb MR, Reeves WH, Chan EK. Upregulated miR-146a expression in peripheral blood mononuclear cells from rheumatoid arthritis patients. Arthritis Res Ther. 2008;10(4): R101
8. Rajasekhar M, Olsson AM, Steel KJ, et al. MicroRNA-155 contributes to enhanced resistance to apoptosis in monocytes from patients with rheumatoid arthritis. J Autoimmun. 2017; 79:53-62.
9. Nazari-Jahantigh M, Wei Y, Noels H, et al. MicroRNA-155 promotes atherosclerosis by repressing Bcl6 in macrophages. J Clin Invest. 2012;122(11):4190-4202.
10. Jablonski KA, Gaudet AD, Amici SA, Popovich PG, Guerau-de-Arellano M. Control of the Inflammatory Macrophage Transcriptional Signature by miR-155. PLoS One. 2016;11(7): e0159724.
11. Yan L, Hu F, Yan X, et al. Inhibition of microRNA-155 ameliorates experimental autoimmune myocarditis by modulating Th17/Treg immune response. J Mol Med (Berl). 2016;94(9):1063-1079.

12. De Smet EG, Van Eeckhoutte HP, Avila Cobos F, et al. The role of miR-155 in cigarette smoke-induced pulmonary inflammation and COPD. Mucosal Immunol. 2020;13(3):423-436.
13. Yu G, Song Y, Xie C, et al. MiR-142a-3p and miR-155-5p reduce methamphetamine-induced inflammation: Role of the target protein Peli1. Toxicol Appl Pharmacol. 2019; 370:145-153.
14. Sadri Nahand J, Moghoofei M, Salmaninejad A, et al. Pathogenic role of exosomes and microRNAs in HPV-mediated inflammation and cervical cancer: A review. Int J Cancer. 2020;146(2):305-320.
15. Liu C, Li N, Liu G. The Role of MicroRNAs in Regulatory T Cells. J Immunol Res. 2020; 2020:3232061.
16. Wen DY, Huang JC, Wang JY, et al. Potential clinical value and putative biological function of miR-122-5p in hepatocellular carcinoma: A comprehensive study using microarray and RNA sequencing data. Oncol Lett. 2018;16(6):6918-6929.
17. Zheng W, Li ZY, Zhao DL, et al. microRNA-26a Directly Targeting MMP14 and MMP16 Inhibits the Cancer Cell Proliferation, Migration and Invasion in Cutaneous Squamous Cell Carcinoma. Cancer Manag Res. 2020; 12:7087-7095.
18. Song Z, Zhang L, Wang Y, et al. Constitutive Expression of miR408 Improves Biomass and Seed Yield in Arabidopsis. Front Plant Sci. 2018; 8:2114.
19. Taheri F, Ebrahimi SO, Shareef S, Reiisi S. Regulatory and immunomodulatory role of miR-34a in T cell immunity. Life Sci. 2020; 262:118209.
20. Guo H, Pu M, Tai Y, et al. Nuclear miR-30b-5p suppresses TFEB-mediated lysosomal biogenesis and autophagy. Cell Death Differ. 2021;28(1):320-336.
21. Wang X, He Y, Mackowiak B, Gao B. MicroRNAs as regulators, biomarkers and therapeutic targets in liver diseases. Gut. 2021;70(4):784-795.
22. Goodwin AJ, Li P, Halushka PV, et al. Circulating miRNA 887 is differentially expressed in ARDS and modulates endothelial function. Am J Physiol Lung Cell Mol Physiol. 2020;318(6): L1261-L1269.
23. Rodriguez A, Vigorito E, Clare S, et al. Requirement of bic/microRNA-155 for normal immune function. Science. 2007;316(5824):608-611.
24. Szczepankiewicz D, Langwiński W, Kołodziejski P, et al. Allergic Inflammation Alters microRNA Expression Profile in Adipose Tissue in the Rat. Genes (Basel). 2020;11(9):1034.
25. Stanczyk J, Pedrioli DM, Brentano F, et al. Altered expression of MicroRNA in synovial fibroblasts and synovial tissue in rheumatoid arthritis. Arthritis Rheum. 2008;58(4):1001-1009.
26. Zhang M, Wang L, Huang S, He X. MicroRNA-223 targets NLRP3 to relieve inflammation and alleviate spinal cord injury. Life Sci. 2020; 254:117796.
27. Ma L, Zhang Y, Hu F. miR-28-5p inhibits the migration of breast cancer by regulating WSB2. Int J Mol Med. 2020;46(4):1562-1570.
28. Zhang Y, Wu X, Wu J, et al. Decreased expression of microRNA-510 in intestinal tissue contributes to post-infectious irritable bowel syndrome via targeting PRDX1. Am J Transl Res. 2019;11(12):7385-7397.
29. Jiang L, Qiao Y, Wang Z, et al. Inhibition of microRNA-103 attenuates inflammation and endoplasmic reticulum stress in atherosclerosis through disrupting the PTEN-mediated MAPK signaling. J Cell Physiol. 2020;235(1):380-393.
30. Oliveira SR, Dionísio PA, Correia Guedes L, et al. Circulating Inflammatory miRNAs Associated with Parkinson's Disease Pathophysiology. Biomolecules. 2020;10(6):945.
31. Faraoni I, Antonetti FR, Cardone J, Bonmassar E. miR-155 gene: a typical multifunctional microRNA. Biochim Biophys Acta. 2009;1792(6):497-505.
32. Mann M, Mehta A, Zhao JL, et al. An NF-κB-microRNA regulatory network tunes macrophage inflammatory responses [published correction appears in Nat Commun. 2018 Aug 16;9(1):3338]. Nat Commun. 2017;8(1):851.
33. Li LC, Okino ST, Zhao H, et al. Small dsRNAs induce transcriptional activation in human cells. Proc Natl Acad Sci U S A. 2006;103(46):17337-17342.
34. Wang XY, Yuan L, Li YL, et al. RNA activation technique and its applications in cancer research. Am J Cancer Res. 2018;8(4):584-593.

35. Dar SA, Kumar M. saRNAdb: Resource of Small Activating RNAs for Up-regulating the Gene Expression. J Mol Biol. 2018;430(15):2212-2218.
36. Zhang J, Lan T, Lu Y. Molecular Engineering of Functional Nucleic Acid Nanomaterials toward In Vivo Applications. Adv Healthc Mater. 2019;8(6): e1801158.
37. Mokhtarzadeh A, Vahidnezhad H, Youssefian L, et al. Applications of Spherical Nucleic Acid Nanoparticles as Delivery Systems. Trends Mol Med. 2019;25(12):1066-1079.
38. Zhu G, Hu R, Zhao Z, et al. Noncanonical self-assembly of multifunctional DNA nanoflowers for biomedical applications. J Am Chem Soc. 2013;135(44):16438-16445.
39. Mei L, Zhu G, Qiu L, et al. Self-assembled Multifunctional DNA Nanoflowers for the Circumvention of Multidrug Resistance in Targeted Anticancer Drug Delivery. Nano Res. 2015;8(11):3447-3460.
40. Zhang L, Zhu G, Mei L, et al. Self-Assembled DNA Immunonanoflowers as Multivalent CpG Nanoagents. ACS Appl Mater Interfaces. 2015;7(43):24069-24074.
41. Hu R, Zhang X, Zhao Z, et al. DNA nanoflowers for multiplexed cellular imaging and traceable targeted drug delivery. Angew Chem Int Ed Engl. 2014;53(23):5821-5826.
42. Kim E, Zwi-Dantsis L, Reznikov N, et al. One-Pot Synthesis of Multiple Protein-Encapsulated DNA Flowers and Their Application in Intracellular Protein Delivery. Adv Mater. 2017;29(26):10.1002/adma.201701086.
43. Lee JH, Ku SH, Kim MJ, et al. Rolling circle transcription-based polymeric siRNA nanoparticles for tumor-targeted delivery. J Control Release. 2017; 263:29-38.
44. Matsuoka T, Yoshimatsu G, Sakata N, et al. Inhibition of NLRP3 inflammasome by MCC950 improves the metabolic outcome of islet transplantation by suppressing IL-1β and islet cellular death. Sci Rep. 2020;10(1):17920.
45. Lübow C, Bockstiegel J, Weindl G. Lysosomotropic drugs enhance pro-inflammatory responses to IL-1β in macrophages by inhibiting internalization of the IL-1 receptor. Biochem Pharmacol. 2020; 175:113864.
46. Sreejit G, Abdel-Latif A, Athmanathan B, et al. Neutrophil-Derived S100A8/A9 Amplify Granulopoiesis After Myocardial Infarction. Circulation. 2020;141(13):1080-1094.
47. Mao L, Kitani A, Hiejima E, et al. Bruton tyrosine kinase deficiency augments NLRP3 inflammasome activation and causes IL-1β-mediated colitis. J Clin Invest. 2020;130(4):1793-1807.
48. Lu Q, Wu R, Zhao M, et al. miRNAs as Therapeutic Targets in Inflammatory Disease. Trends Pharmacol Sci. 2019;40(11):853-865.
49. Chen R, Wang T, Rao K, et al. Up-regulation of VEGF by small activator RNA in human corpus cavernosum smooth muscle cells. J Sex Med. 2011;8(10):2773-2780.
50. Guo X, Feng L, Jia J, et al. Upregulation of VEGF by small activating RNA and its implications in preeclampsia. Placenta. 2016; 46:38-44.

Figures

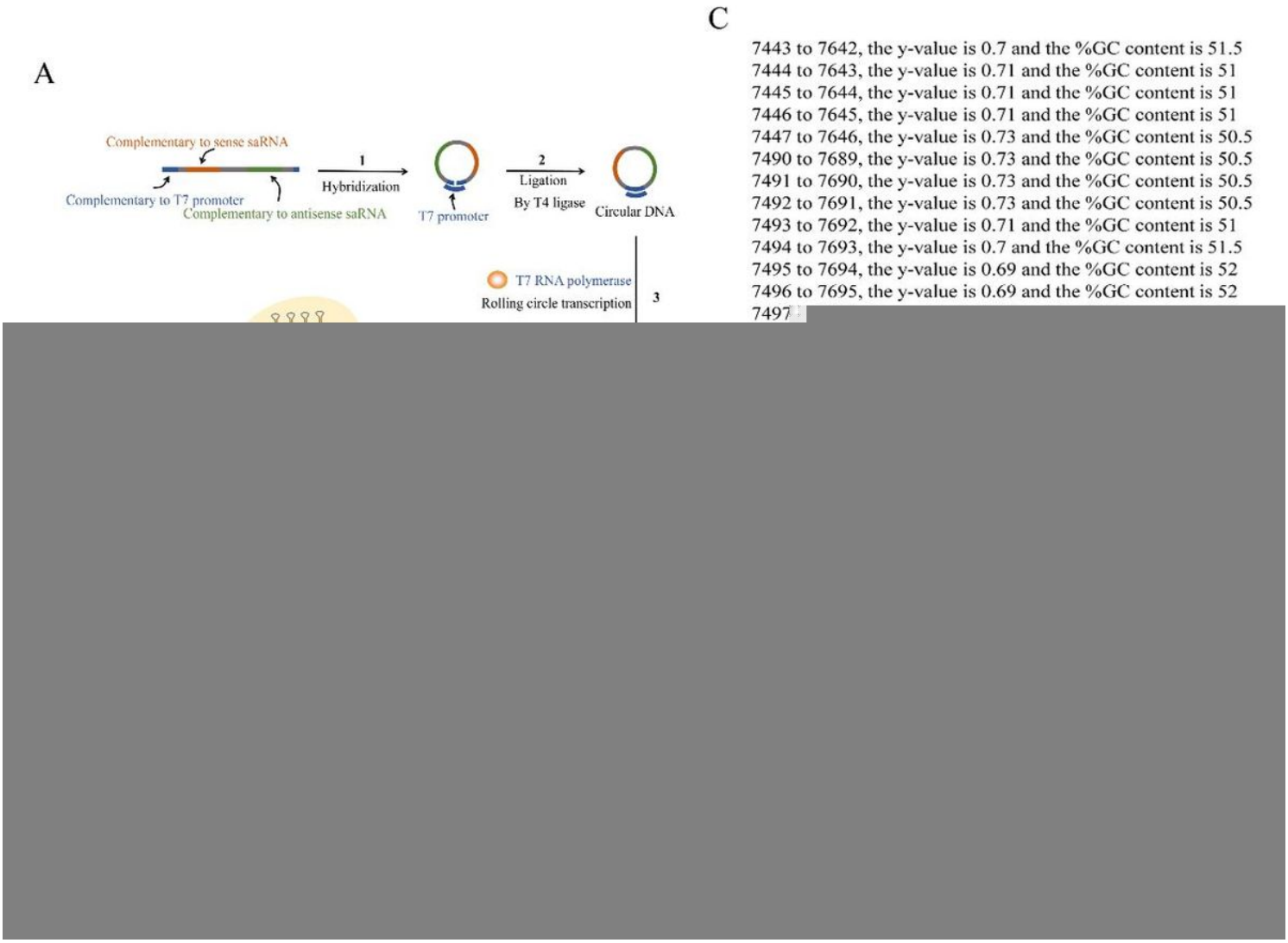

Figure 1

Design of NFs that can activate miR-155. (A) Schematic illustration of the preparation of NFs using rolling circle transcription (RCT). (B) The transcription start site of 10,000 bases upstream from the 5'end of the first exon of MiR155HG. (C) The enriched region of CpG islands.

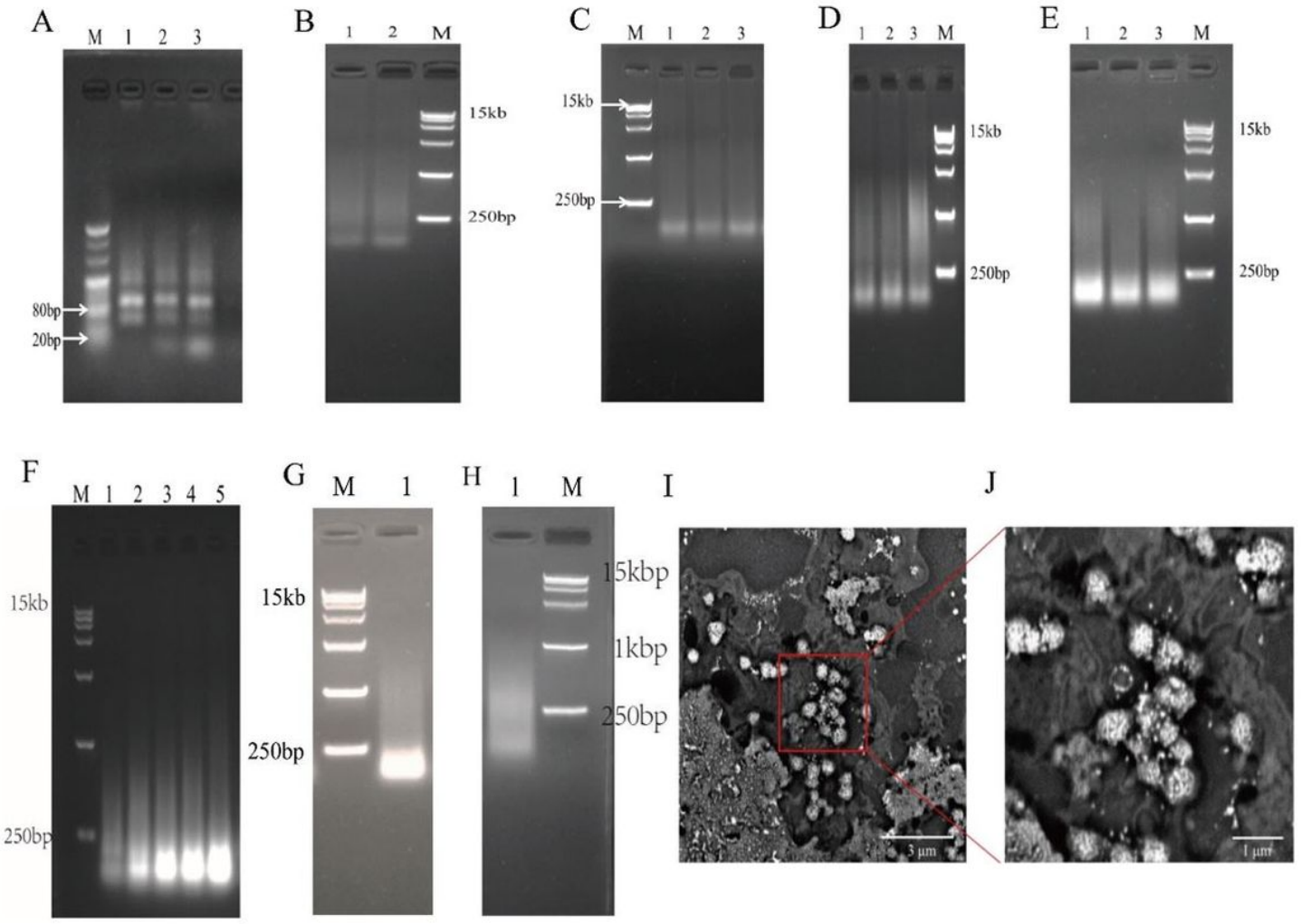

Figure 2

RCT reaction system optimization and NFs characterization. (A) Different concentration ratios of template and primer were used to perform the hybridization and ligation reactions. Lane M: marker, from top to bottom: 500 bp, 400 bp, 300 bp, 200 bp, 100 bp, 80 bp, and 20 bp; lanes 1–3: template to primer concentration ratios of 1:1, 1:2, and 1:3. (B) Various ligases were used for amplification. Lane M: marker, from top to bottom: 15 kb, 1 kb, 7,500 bp, 5,000 bp, 2,500 bp, 1,000 bp, and 250 bp; lane 1: Taq DNA ligase was used; lane 2: T4 DNA ligase was used. (C–E) Products amplified with different hybridization times and ligation times. Lane M: Marker, from top to bottom, 15 kb, 1 kb, 7,500 bp, 5,000 bp, 2,500 bp, 1,000 bp, and 250 bp; (C) lanes 1–3: hybridization time 1 h, ligation time: 1 h, 2 h, 3 h. (D) Lanes 1–3: hybridization time 2 h, ligation time: 1 h, 2 h, 3 h. (E) Lanes 1–3: hybridization time 3 h, ligation time: 1 h, 2 h, 3 h. (F) Different concentrations of rNTPs were used for transcription. Lane M: marker, from top to bottom: 15 kb, 1 kb, 7,500 bp, 5,000 bp, 2,500 bp, 1,000 bp, and 250 bp; lanes 1–5: rNTP concentrations of 2 mM, 4 mM, 6 mM, 8 mM, and 10 mM. (G, H) Amplification products before and after rolling circle transcription system optimization. Lane 1: RNA; lane M: marker. (I, J) SEM images of the NFs.

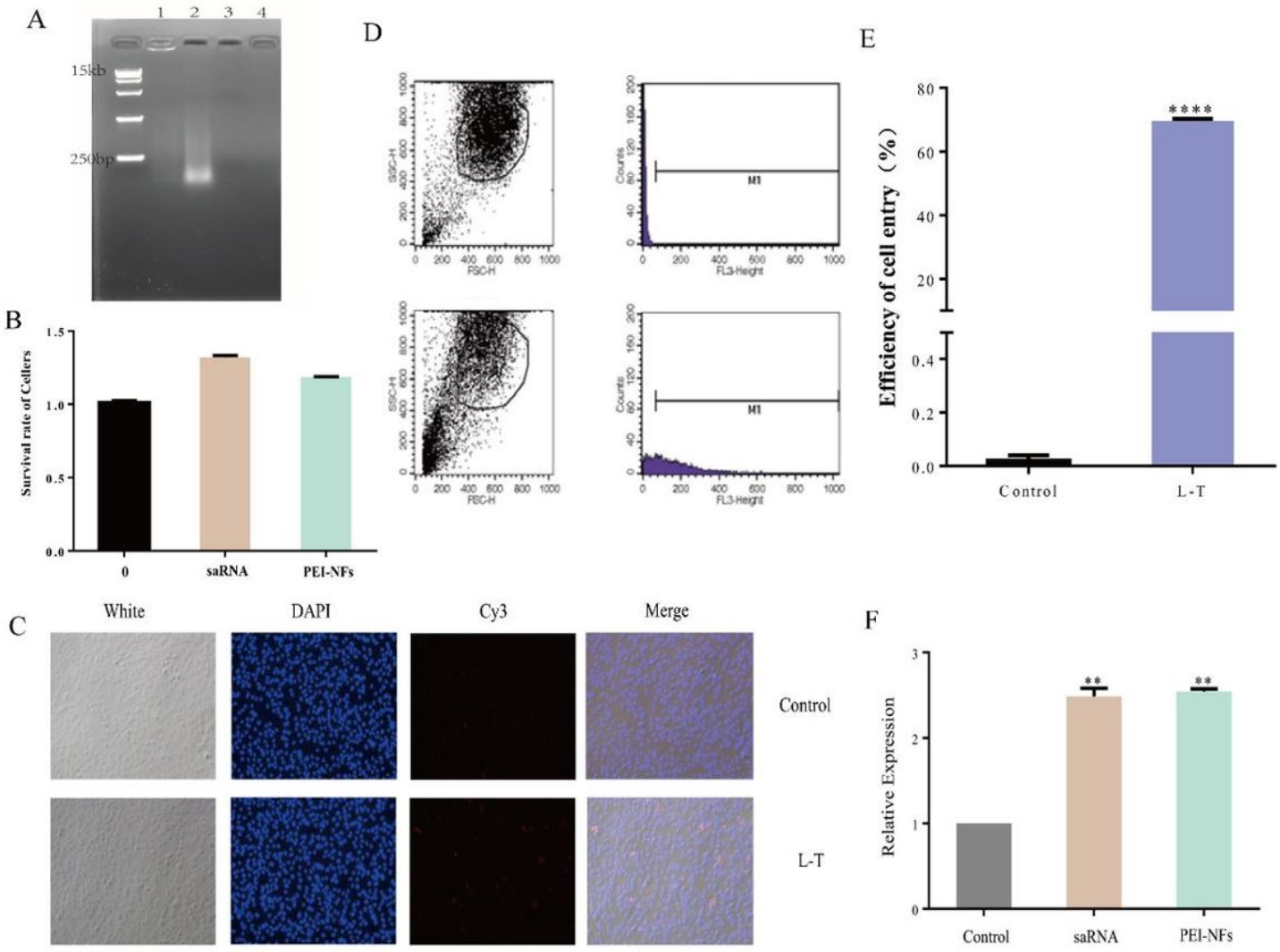

Figure 3

(A) Gel image of the product after the complexation of NFs and PEI. Lane 1: PEI-NFs complexes; lane 2: NFs; lane 3: PEI; lane 4: negative control. (B) Cellular viability of HUVECs exposed to saRNA and PEI-NFs for 24 h. “0” represents the control. (C) Fluorescence imaging of cells treated with PEI-NF complex for 24 h (magnification, 10×). (D) Flow plots at 12 h after the NFs entered the cells. Results for the control group and experimental group are shown. (E) Efficiency of PEI-NF delivery into cells after 12 h (****P < 0.0001). (F) Relative VEGF expression in cells treated with saRNA or PEI-NFs complex for 72 h (**P < 0.01 vs. control).

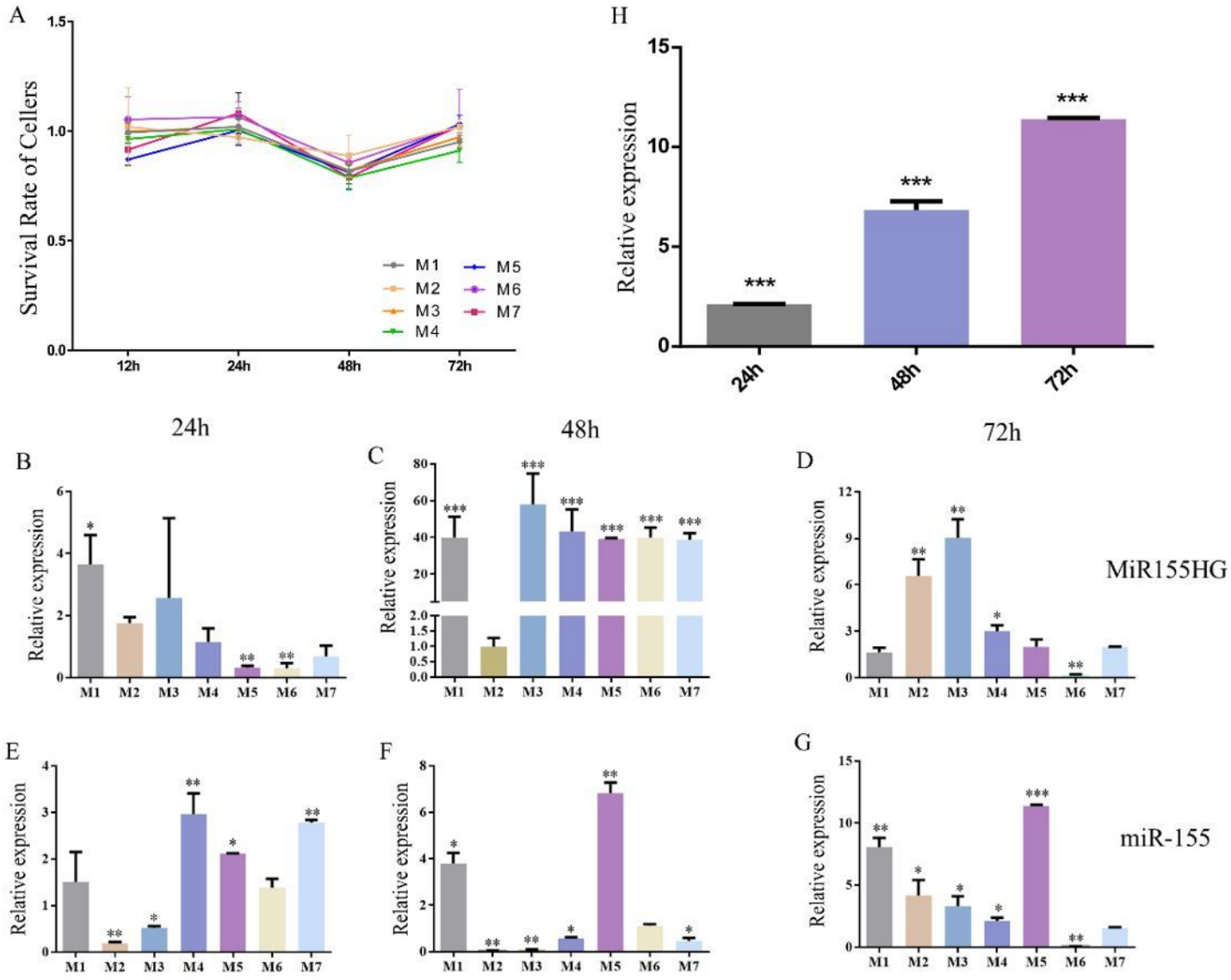

Figure 4

(A) NFs M1–M7 were prepared from different saRNA template sequences. Cell survival rates after 12, 24, 48, or 72 h were determined using the CCK-8 assay. P > 0.05 vs. control. (B–D) Relative MiR155HG expression levels at 24 h, 48 h, or 72 h after treatment of HUVECs with NFs M1–M7. (E-G) Relative miR-155 expression levels at 24 h, 48 h, or 72 h after treatment of HUVECs with NFs M1–M7. (H) Relative miR-155 expression in HUVECs treated with M5 for 24 h, 48 h, or 72 h.

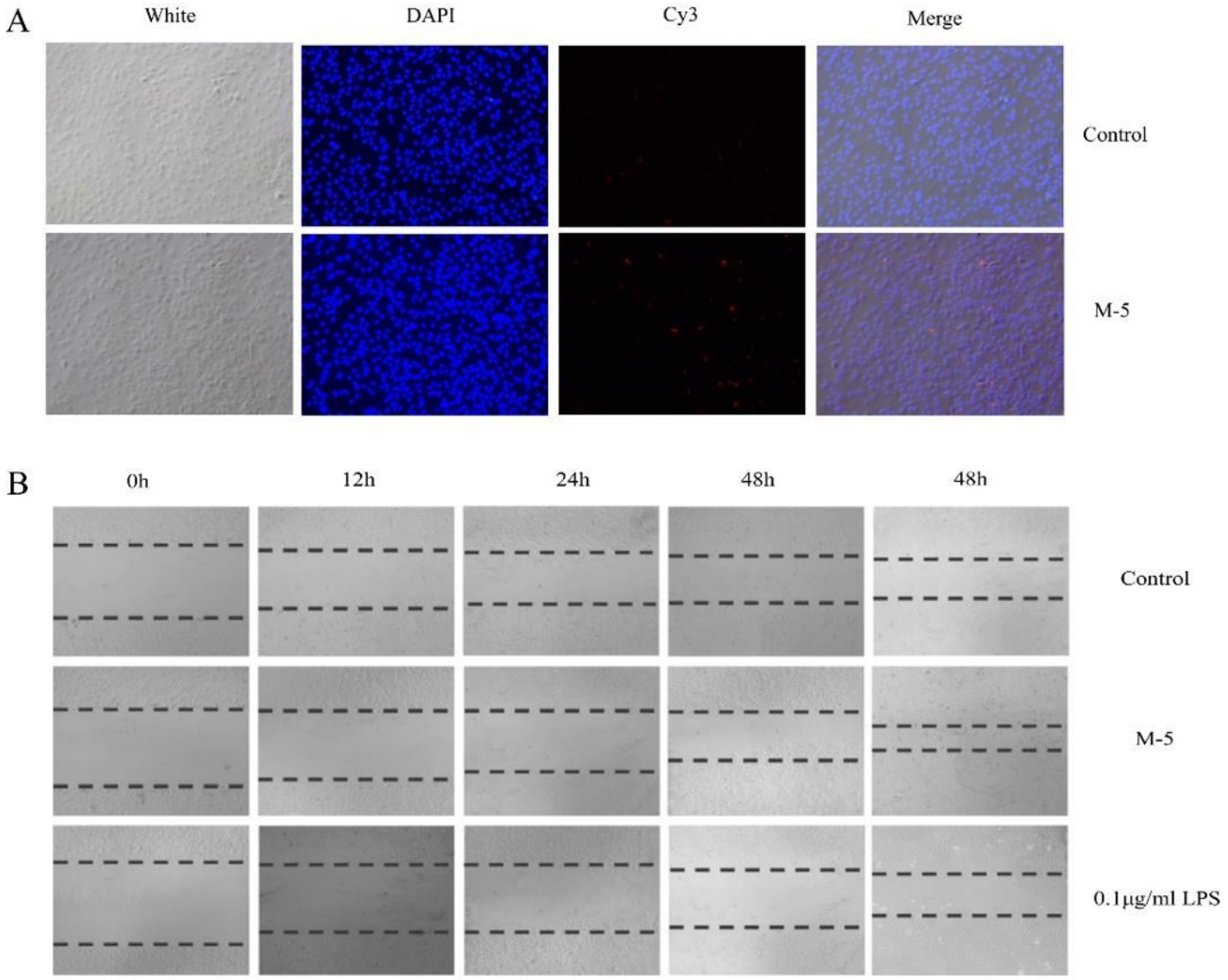

Figure 5

(A) Fluorescence imaging of cells after treatment with NFs (M5) for 24 h (magnification, 10×). (B) Results of scratch assays of cells treated with NFs (M5) at 0 h, 12 h, 24 h, 48 h, and 72 h (10×).

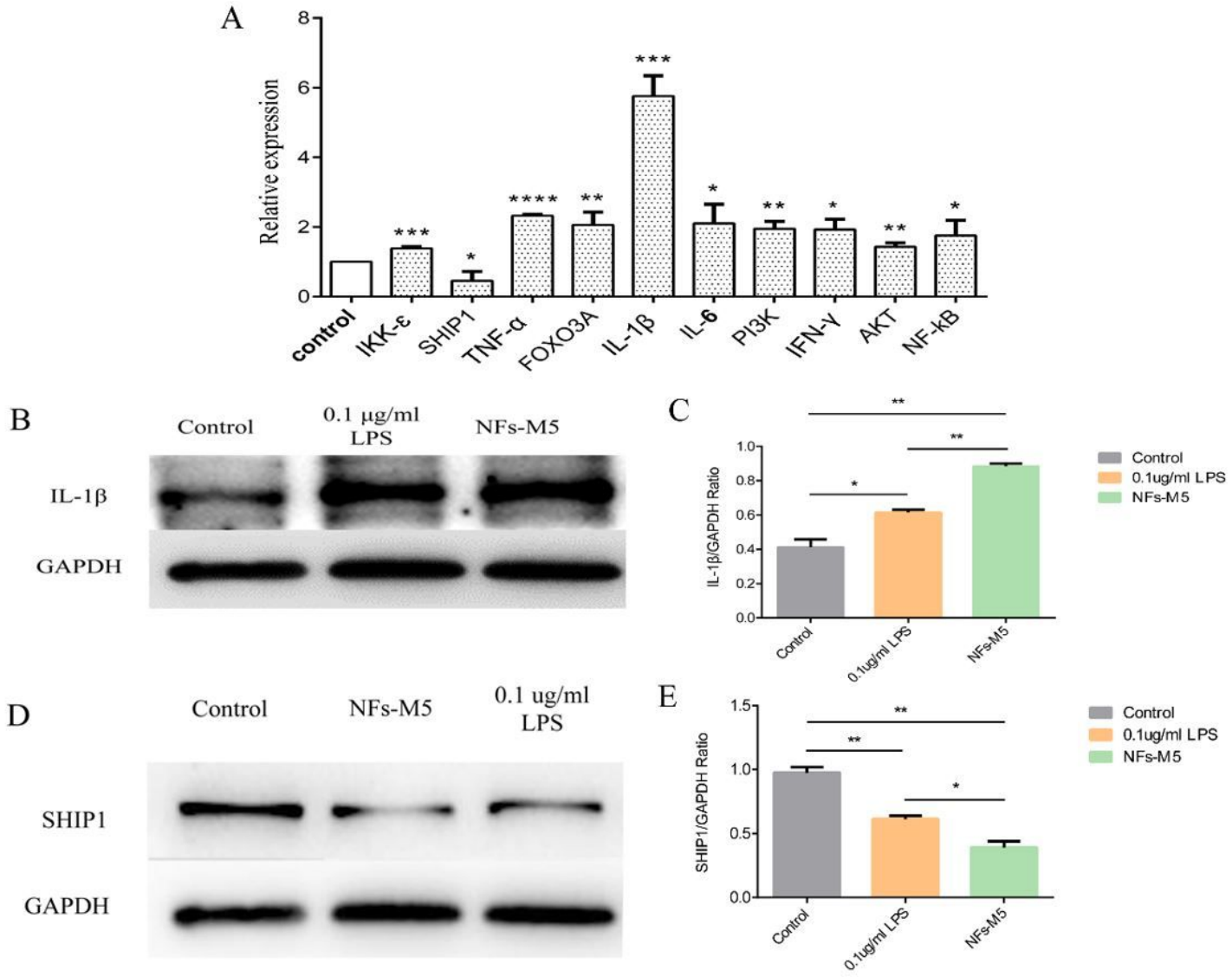

Figure 6

(A) Relative gene expression levels of inflammation-related factors (IKK□, SHIP1, TNF-α, FOXO3A, IL-1β, IL-6, PI3K, IFN-γ, AKT, and NF-κB) 72 h after treatment of HUVECs with NFs (M5) as determined by RT-qPCR. (B) Western blot analysis of IL-1β protein expression in cells treated with 0.1 μg/mL LPS or NF-M5 for 72 h. (C) Relative IL-1β protein levels (expression levels were normalized to that of GAPDH). (D) Western blot analysis of SHIP1 protein expression in cells treated with 0.1 μg/mL LPS or NF-M5 for 72 h. (E) Relative SHIP1 protein levels (expression levels were normalized to that of GAPDH).

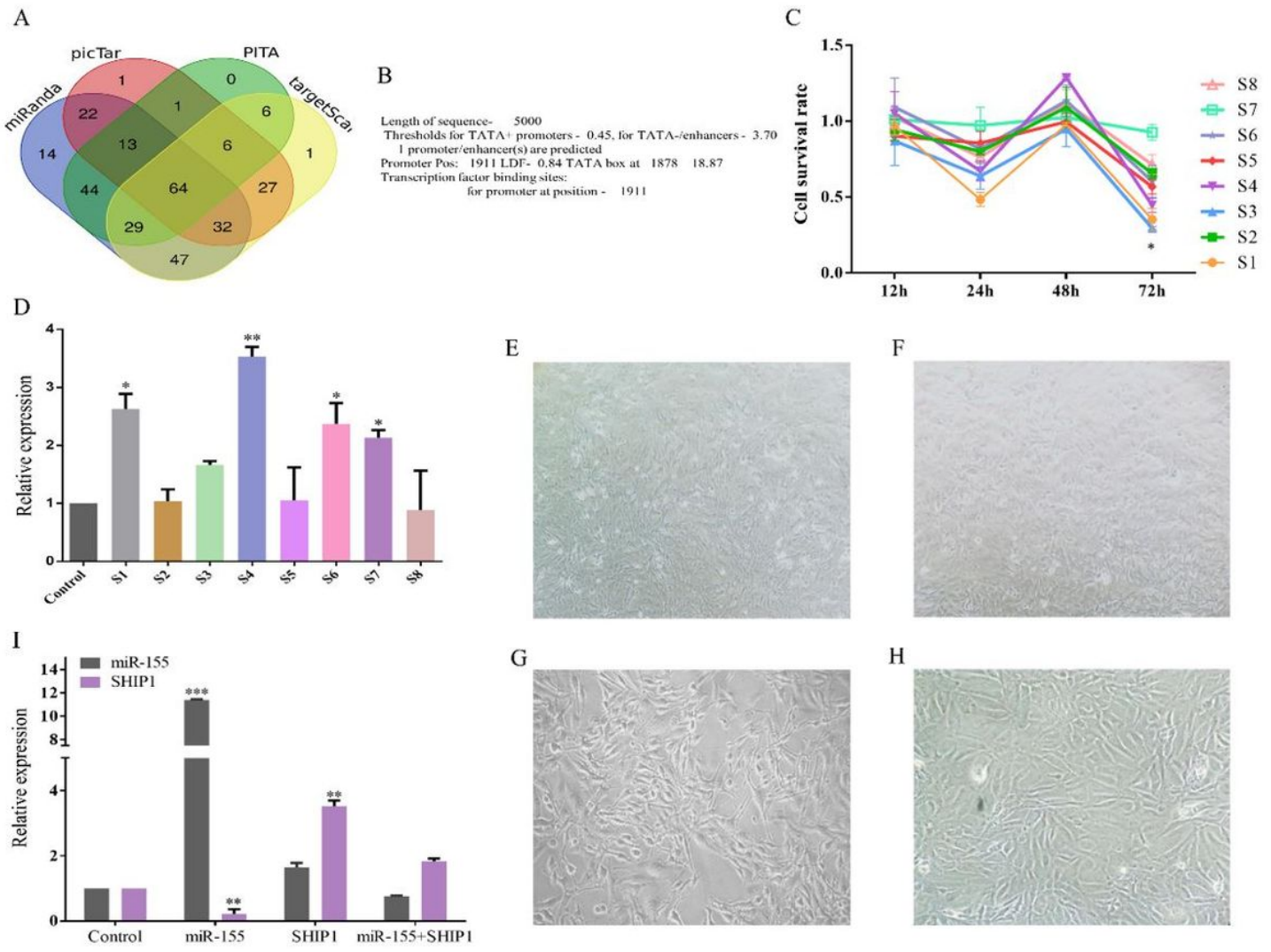

Figure 7

(A) Relationships between the numbers of miR-155 target genes predicted by the four tools used in this study. (B) Prediction of the transcription start site in the 5,000 bases upstream of the 5' end of the first exon of INPP5D. (C) Cell survival rates of HUVECs treated with nucleic acid NFs S1–S8 activating SHIP1 at 12 h, 24 h, 48 h, and 72 h (*P < 0.05 vs. control). (D) SHIP1 expression in cells treated with nucleic acid NFs S1–S8 for 72 h (*P < 0.05 vs. control; **P < 0.01 vs. control). (E) Control cells cultured in the absence of NFs (magnification,4×). (F) Cell state at 72 h after miR-155 expression activation (magnification, 4×). (G) Cell state at 72 h after SHIP1 expression activation (magnification,10×). (H) Simultaneous activation of miR-155 and SHIP1 expression (magnification,10×). (I) Relative expression levels of SHIP1 and miR-155 in HUVECs treated with NF-M5, NF-S4, NF-M5, and NFs-S4 for 72 h (**P < 0.01 vs. control; ***P < 0.001 vs. control).

Supplementary Files

This is a list of supplementary files associated with this preprint. Click to download.

- SupplementaryDate1.docx
- SupplementaryDate2.docx
- SupplementaryTable.docx
- SupplementaryFigure.docx